Effects of change of the cation M^{2+} on crystal structure and optical properties of divalent samarium-doped $MAl_2Si_2O_8$ (M=Ca, Sr, Ba)

Ling Li*, Xiaoguang Liu*

Ministry-of-Education Key Laboratory for the Synthesis and Applications of Organic Functional Molecules, Hubei Collaborative Innovation Center for Advanced Organochemical Materials, Hubei University, Wuhan 430062, China

*Corresponding author: Tel +86-27-88662747; fax +86-27-88663043

E-mail addresses: Ling Li: liling402431@hotmail.com;

Xiaoguang Liu: liuxiaoguang402@hotmail.com;

Abstract

In order to investigate the effects of cation ion change on crystal structure and optical properties of divalent samarium-doped $MAl_2Si_2O_8$, the Sm^{2+} doped triclinic $CaAl_2Si_2O_8$ (CASO), monoclinic $SrAl_2Si_2O_8$ (SASO) and $BaAl_2Si_2O_8$ (M-BASO) as well as hexagonal $BaAl_2Si_2O_8$ (H-BASO) have been synthesized using polymerizable-complex technique under reducing atmosphere. At room temperature, under the N-UV or blue excitation, Sm^{2+} doped SASO, M-BASO and H-BASO showed strong red emission, which widen the group of novel red-emitting materials. Their emission bands of Sm^{2+} consists of a broad 4f-5d transition band and sharp f-f transition lines. The correlation between the crystal structure and the 4f-4f transition emission intensity of Sm^{2+} as well as the excitation peaks

of 5d energy level is deeply discussed, and the theoretical analysis is in good agreement with our experimental result. These are essential to understand the relationship between the crystal structure and luminescence properties, which are fundamental to design luminescent materials of Sm systems.

1. Introduction

The alkaline-earth feldspars $MAl_2Si_2O_8$ (M=Ca, Sr, Ba) were reported to be very suitable host lattices for the luminescent divalent rare earth ion especially the Eu^{2+} ions[1-8]. Among the various rare earth ions, Sm^{2+} doped inorganic materials have been found important applications in lighting, display and persistent spectral hole-burning (PSHB)[9-13]. Sm^{2+} ions doped inorganic materials have been attracted more and more attention because they have the advantages of 4f-5d broad excitation and emission bands as well as the sharp f-f transition emission[9-14]. The Sm^{2+} generally has a broad continuum excitation band in the range from 200 to 500 nm. And its emission is composed of the 4f-5d broad band and deep red $4f^6$-$4f^6$ sharp emission. However, optical properties of Sm^{2+} doped alkaline-earth feldspars $MAl_2Si_2O_8$ (M=Ca, Sr, Ba) have not been reported.

On the other hand, the luminescence of divalent samarium ions is sensitive to the crystalline environment of the lattice site that it occupies[15]. The relative position between the lowest-lying $4f^5 5d^1$ excited states and the $4f^6$ ($^5D_0$) level governs whether the emission displays $4f^6 \rightarrow 4f^6$ sharp line and/or $4f^55d^1 \rightarrow 4f^6$ broad band. It has been reported that the 4f-5d excited broad band is dependent on many factors such as the crystal field strength, the coordination number and the covalence of the bonds[10]. Understanding the relationship between these factors and the 4f-5d transition of Sm^{2+} is of great importance due to the potential technological applications as functional photonic materials. We will choose the systematic alkaline-earth feldspars $MAl_2Si_2O_8$ (M=Ca, Sr, Ba) as the host lattices to investigate the effects of the crystal structure on the 4f-5d excitation band due to their characteristic structural properties. In these host lattices, firstly, the number of the M^{2+} site occupied by Sm^{2+} is different. In $CaAl_2Si_2O_8$, Ca^{2+} includes four different 2i sites[16], but only one kind of M^{2+} (Sr^{2+} or Ba^{2+}) site exists in the SASO[17], M-BASO[18] and H-BASO[4]. So the effects of the number of the occupied sites on the 4f-5d transition can be obtained. Secondly, the symmetry of the M^{2+} is different. The Ba^{2+} site of H-BASO is central symmetry while the others are non-central symmetry. Thus the effects of the symmetry on the photoluminescence properties of Sm^{2+} can be shown. Thirdly, the SASO is monoclinic and isostructural with the M-BASO. They are similar to each other except the different cation site. So the effects of the cation ions on the 4f-5d of Sm^{2+} can be obtained. Fourthly, the H-BASO and the M-BASO are allomorphism. They are different in crystalline form without change in chemical constitution. So the effects the crystal structure with the same chemical constitution on the f-d transition peak can be investigated.

In order to obtain more exact photoluminescence data and high-efficiency phosphor emission, it is necessary to utilize solution-based techniques for synthesis. We used Pechini-type sol-gel process[19] (PSG, also known and called as polymerizable-complex technique) to synthesize the Sm doped $MAl_2Si_2O_8$ (M=Ca, Sr, Ba). If precursor powders are prepared using PSG, all the component ions can be evenly dispersed in the precursors, leading to the formation of high-purity phosphors with a uniform dispersion of Sm ions activators.

In our paper, the Sm^{2+} doped triclinic $CaAl_2Si_2O_8$ (CASO), monoclinic $SrAl_2Si_2O_8$ (SASO) and $BaAl_2Si_2O_8$ (M-BASO) as well as hexagonal $BaAl_2Si_2O_8$ (H-BASO) have been synthesized using polymerizable-complex technique under reducing atmosphere. The photoluminescence properties of Sm^{2+} in the systematic host lattices have been reported. Furthermore, the important chemical bonds such as the environmental factor (h_e) and parameter (F_C) were calculated using the dielectric theory of complex crystals. The effects of the crystal structure on the 4f-5d transition and f-f emission intensity of Sm^{2+} were discussed.

2. Experimental section

2.1. Sample Preparation: Unless otherwise stated, all reagents were purchased from Sigma-Aldrich. The $MAl_2Si_2O_8$ (M=Ca, Sr, Ba) powder samples were prepared by a pechini-type sol-gel process (PSG, also known and called as polymerizable-complex technique), which can give the highest possible homogeneity for the material[19]. The doping level of Sm ions was 5.0 mol % in $MAl_2Si_2O_8$:Sm. The mixtures were heated in a hydrogen-nitrogen (5%H_2+95% N_2) atmosphere.

The raw materials were Sm_2O_3, $Ca(NO_3)_2 \cdot 4H_2O$, $Ba(NO_3)_2$, $Sr(NO_3)_2$, $Al(NO_3)_3 \cdot 9H_2O$, tetraethyl orthosilicate ($Si(OC_2H_5)_4$, TEOS) and citric acid as the chelating agent. The 0.05M $Sm(NO_3)_3$ solution was prepared by dissolving Sm_2O_3 in the diluted HNO_3 and adding appropriate volume of de-ionized water. The 0.25M $M(NO_3)_2$ (M=Ca, Sr, Ba), $Al(NO_3)_3$ solutions and 1M citric acid solution were prepared using the de-ionized water. Briefly, a stoichiometric volumes of $M(NO_3)_2$ (M=Ca, Sr, Ba) and $Al(NO_3)_3$ solutions were dissolved in an aqueous solution of citric acid (citric acid/M^{2+}=2:1, molar ratio) under vigorous stirring to form solution “A”. Then TEOS was dissolved using some ethanol under stirring to form solution “B”. Then A and B were mixed together and stirred for several hours at room temperature. The resultant mixture was heated up to 120 ℃ and kept at the temperature for 4 h to produce solid gels. The solid gels were prefired at 1200℃ for 4 h. After being fully ground, Sm: M-BASO (M=Ca, Sr) samples were annealed at 1400℃ in the reducing atmosphere for 6 h and single hexagonal and monoclinic phases of Sm: BASO were obtained between 1350 to 1650 ℃ in the reducing atmosphere for 6 h.

2.2. Characterizations

The phase purity of the as prepared phosphor was checked by powder x-ray diffraction (XRD) analysis by using a D/MAX 2500 instrument (Rigaku) with a Rint 2000 wide angle goniometer and Cu Kα1 radiation (λ =1.54056 A) at 40 kV and 100 mA. The measurements of photoluminescence (PL) and photoluminescence excitation (PLE) spectra were performed by using a fluorescence spectrophotometer (Photon Technology International) equipped with a 60 W Xe-arc lamp as the excitation light source. All the measurements were taken at room temperature.

3. Theoretical method

The dielectric theory of complex crystals was used to calculate the chemical bond parameters of inorganic compounds quantitatively[20-24]. In this theory, the complex crystals with crystal formula $A_{a_1}^1 A_{a_2}^2 \cdots A_{a_i}^i B_{b_1}^1 B_{b_2}^2 \cdots B_{b_j}^j$ can be written as a linear combination of the sub-formula of various binary crystals when the crystal structure is known. The sub-formula of any type of chemical bond A-B in the multi-bond crystal $A_{a_1}^1 A_{a_2}^2 \cdots A_{a_i}^i B_{b_1}^1 B_{b_2}^2 \cdots B_{b_j}^j \ldots$ can be expressed by the following formula:

$$\frac{N_{(B^j - A^i)} \times a_i}{N_{CA^i}} A^i \frac{N_{(A^i - B^j)} \times b_j}{N_{CB^j}} B^j = A_{m_i}^i B_{n_j}^j \qquad (1)$$

where

$$m_i = \frac{N_{(B^j - A^i)} \times a_i}{N_{CA^i}}, n_j = \frac{N_{(A^i - B^j)} \times b_j}{N_{CB^j}} \qquad (2)$$

And the bond sub-formula equation is given by:

$$A^1_{a_1} A^2_{a_2} \cdots A^i_{a_i} B^1_{b_1} B^2_{b_2} \cdots B^j_{b_j} = \sum_{i,j} A^i_{m_i} B^j_{n_j} \qquad (3)$$

where $A^i_{a_i}$, $B^j_{b_j}$ stands for the different constituent elements or different sites of the same element in the crystal formula, and a_i, b_j represents the number of the corresponding element. $N_{(B^j\text{-}A^i)}$ is the number of B^j ions in the coordination group of a A^i ion, and N_{CA^i} represents the nearest coordination number of A^i ion. This means that the complex crystal is decomposed into the sum of different binary crystals like $A^i_{m_i} B^j_{n_j}$.

Once the different binary crystals are obtained, the covalency of any μ type binary bond can be defined as[25]:

$$f_c^\mu = \frac{E_h^{\mu 2}}{E_g^{\mu 2}} \qquad (4)$$

where

$$(E_g^\mu)^2 = (E_h^\mu)^2 + (C^\mu)^2 \qquad (5)$$

and

$$E_h^\mu = 39.74/(d^\mu)^{2.48} \qquad (6)$$

$$C^\mu = 14.4 b^\mu \exp(-k_s^\mu . r_0^\mu)[(Z_A^\mu)^* - \frac{n}{m}(Z_B^\mu)^*]/r_0^\mu \quad (n > m) \qquad (7)$$

$$C^\mu = 14.4 b^\mu \exp(-k_s^\mu . r_0^\mu)[\frac{m}{n}(Z_A^\mu)^* - (Z_B^\mu)^*]/r_0^\mu \quad (n < m) \qquad (8)$$

Here, d^μ is the bond distance (in Å) and r_0^μ is half of the bond distance. k_s^μ is the Thomas-Fermis screening wavenumber of valence electrons and α_B is the Bohr radius. b^μ is proportional to the square of the average coordination number. $(Z_A^\mu)^*$ and $(Z_B^\mu)^*$ are the number of effective valence electrons of the cation and anion in the μ type bond, respectively.

For the chemical bond of type μ, the polarizable coefficient α_0^μ can be obtained from the Lorentz-Lorenz equation

$$\left(\varepsilon^\mu - 1\right)\Big/\left(\varepsilon^\mu - 2\right) = \left(4\pi/3\right)\alpha_0^\mu \quad (9)$$

Hence, the polarizability of the chemical bond volume ($Å^3$) is given by:

$$\alpha_b^\mu = \alpha_0^\mu v_b^\mu \quad (10)$$

More detail calculation process can be referred to the reference[25].

4. Result and discussion

4.1.Crystal Phase Formation

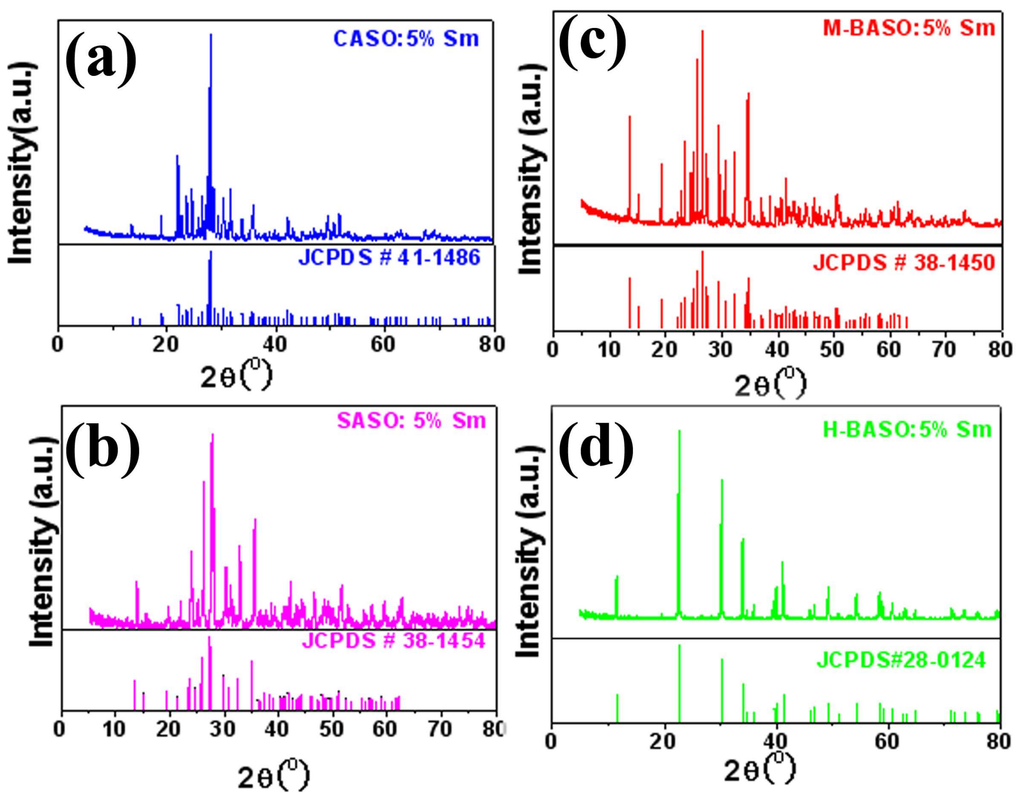

Figure 1. XRD patterns of Sm-doped $MAl_2Si_2O_8$ samples prepared in reducing

atmosphere. (a) $CaAl_2Si_2O_8$:Sm; (b) $SrAl_2Si_2O_8$:Sm; (c) monoclinic $BaAl_2Si_2O_8$:Sm; (d) hexagonal $BaAl_2Si_2O_8$:Sm

Figure 1. shows X-ray diffraction (XRD) patterns of Sm-doped $MAl_2Si_2O_8$ samples prepared in reducing atmosphere. It is clear that all the diffraction peaks of four Sm-doped compounds can be readily indexed to the corresponding standard data for triclinic phase of $CaAl_2Si_2O_8$ (JCPDS 48-1454), monoclinic phase of $SrAl_2Si_2O_8$ (JCPDS 38-1454) and $BaAl_2Si_2O_8$ (JCPDS 38-1450) as well as the hexagonal phase of $BaAl_2Si_2O_8$ (JCPDS 28-0124), respectively. No other impurities can be detected. In addition, the refined crystallographic unit cell parameters of the calcined products were calculated using the software Jade 5.0 and listed in Table 1.

Table 1: Unit cell parameters of Sm-doped $MAl_2Si_2O_8$ samples

compound	a(Å)	b (Å)	c (Å)	α (°)	β(°)	γ(°)
H-BASO:5%Sm	5.2942	5.2942	7.7836	90	90	120
Pure H-BASO[a]	5.2955	5.2955	7.7817	90	90	120
M-BASO:5%Sm	8.6316	13.0444	14.4053	90	115.11	90
Pure M-BASO[b]	8.6268	13.045	14.408	90	115.22	90
SASO:5%Sm	8.3705	12.9671	14.2559	90	115.25	90
Pure SASO[c]	8.392	12.967	14.260	90	115.43	90
CASO:5%Sm	8.16785	12.87079	14.17677	93.2473	115.731	91.1248
Pure CASO[d]	8.173	12.869	14.165	93.113	115.913	91.261

[a] reference 4; [b] reference 18 ; [c] reference 17; [d] reference 16

4.2. Photoluminescence Properties.

The photoluminescence properties of Sm^{2+} in different host lattices are quite different because of their different environmental factor. Divalent Sm^{2+} has the $4f^6$ electron configuration. Under irradiation with UV to blue light, it can be excited into the $4f^55d^1$ continuum, from which the ions rapidly relax to the lowest excited state[9-13]. Just as the Eu^{2+} or Ce^{3+} ions, the f-d luminescence wavelength of phosphors employing Sm^{2+} changes greatly with the type of the host crystal[1, 26].

4.2.1. Characteristic luminescence of Sm^{2+} in $MAl_2Si_2O_8$ (M=Ca, Sr, Ba):Sm

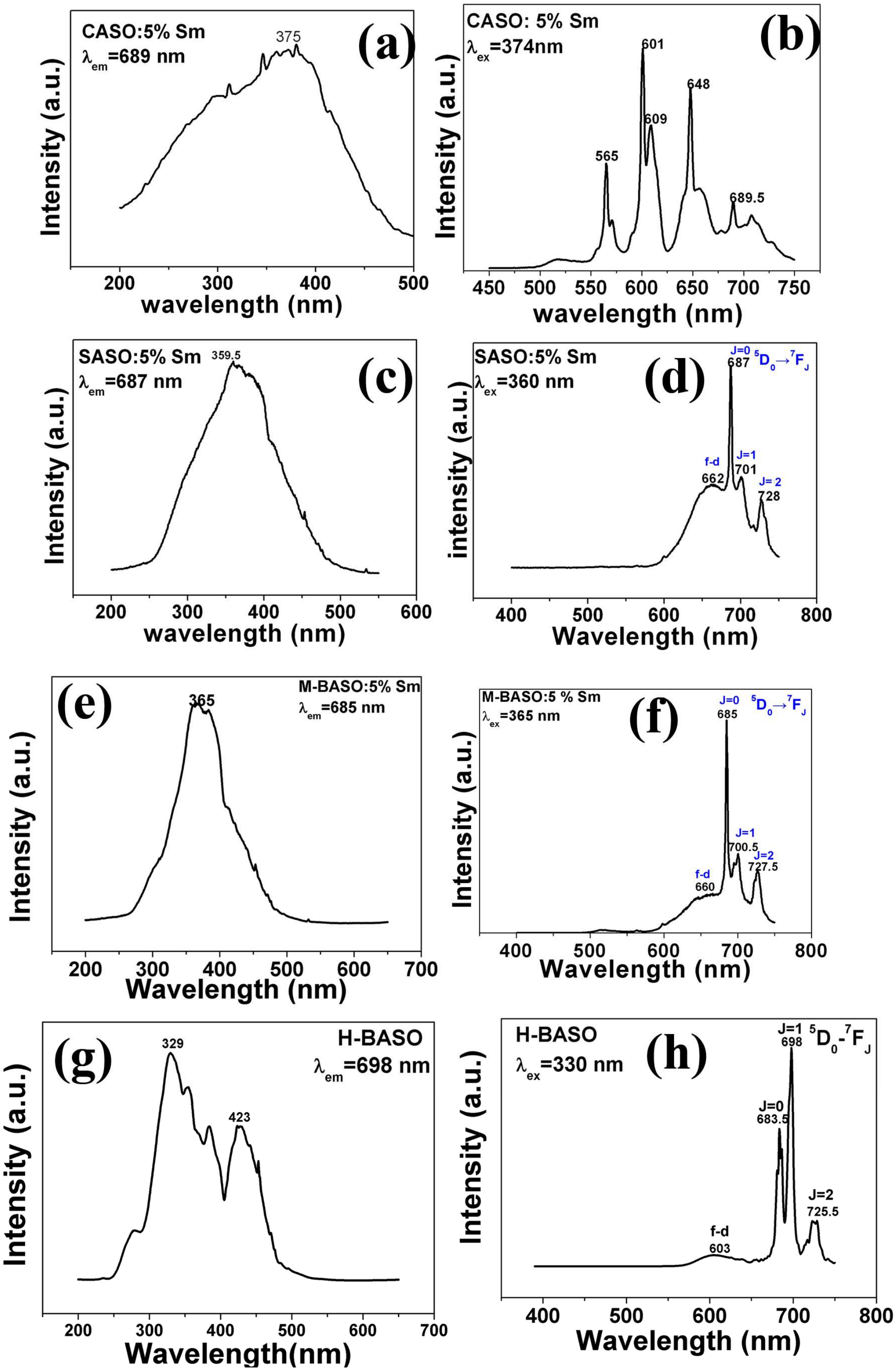

Figure 2. Photoluminescence emission and excitation spectra of Sm-doped $MAl_2Si_2O_8$ (M= Ba, Sr, Ca)samples related to the luminescence centre ions Sm^{2+} at room temperature.

Figures 2 shows the excitation and emission spectra of Sm doped

CASO, SASO, M-BASO and H-BASO samples at room temperature with the initial samarium concentration of 5 mol%. Different excitation wavelength produces different photoluminescence spectra. For CASO:Sm, Figure 2(a) shows the broad excitation band monitored by 689 nm with the peak at 375 nm. In the emission spectra under the excitation at 375 nm, a weaker $^5D_0\rightarrow^7F_0$ transition of Sm^{2+} at 698.5 nm can be found (Figure 2(b)).Unusual luminescence of Sm^{3+} in CASO can be monitored. As can be shown in Figure 2(b), the sharp emission lines at 565, 601, 648 nm come from the f-f transitions of Sm^{3+}, which can be assigned to $^4G_{5/2}\rightarrow^6H_{5/2}$, $^4G_{5/2}\rightarrow^6H_{7/2}$, $^4G_{5/2}\rightarrow^6H_{9/2}$, respectively. It indicates the existence of Sm^{3+} in CASO.

Figures 2(d), 2(f) and 2(h) show that Sm doped SASO, M-BASO and H-BASO samples exhibit efficient deep red emission under irradiation with UV light. For SASO: Sm, the excitation spectrum (Figure 2(c), λ_{ex}=687 nm) consists of a broad band from 250 to 500 nm with a maximum at 359.5 nm. This is assigned to 4f-5d transition of Sm^{2+}. As is shown in Figure 2(d), under the excitation into the $4f^55d^1$ states with the wavelength at 360 nm, the obtained emission spectra of SASO: Sm show a broad band emission from 600 to 750 nm overlapped with the f-f transitions of Sm^{2+}. The peak of the broad band emission is 662 nm assigned to f-d transition of Sm^{2+}. The sharp emission bands consists of three groups of lines at 687, 702 and 727 nm corresponding to the

$^5D_0 \rightarrow ^7F_0$, $^5D_0 \rightarrow ^7F_1$ and $^5D_0 \rightarrow ^7F_2$ transitions of Sm^{2+}, respectively. The dominant line is about 687 nm ($^5D_0 \rightarrow ^7F_0$ transition of Sm^{2+} ions), which shows that Sm^{2+} ions occupy the crystallographic sites without central symmetry in the host.

Table 2. The excitation and emission peak positions of Sm^{2+} in the samples $MAl_2Si_2O_8$: 5% Sm (M= Ba, Sr, Ca) ("*" indicates the strongest peak position of the excitation and emission spectra.)

Sample	Excitation (f→d) (nm)	Emission (nm)			
		d→f	f-f transition ($^5D_0 \rightarrow ^7F_J$)		
			J=0	J=1	J=2
CASO:Sm	375*	-	689.5*	-	-
SASO:Sm	359.5*	662	687*	702	727
M-BASO:Sm	365*	660	685*	700.5	727.5
H-BASO:Sm	329* 423*	603	683.5	698*	725.5

The excitation and emission spectra of M-BASO:Sm show in Figure 2(e) and 2(f). The broad excitation band with the peak at 365 nm extends from 250 to 500 nm. And the broad f-d transition emission of Sm^{2+} ranges from 600 to 750 nm with the peak at 660 nm. The sharp emission bands consists of three groups of lines at 685, 700.5 and 727.5 nm corresponding to the $^5D_0 \rightarrow ^7F_0$, $^5D_0 \rightarrow ^7F_1$ and $^5D_0 \rightarrow ^7F_2$ transitions of Sm^{2+}, respectively. The optical properties of M-BASO:Sm are similar to those of SASO: Sm. This is because that the crystal structure of M-BASO is close to that of SASO:Sm , thus crystal environment of Sm^{2+} in M-BASO is near to SASO:Sm. However, compared with that of SASO:Sm, a red-shift of the excitation for M-BASO:Sm can be found and the reason will be discussed in the discussion part.

As can be shown in Figures 2(g) and 2(h), the sample H-BASO:Sm shows different excitation and emission spectra. The spectra are quite different with the photoluminescence properties of Sm doped SASO and M-BASO samples. Two dominate excitation peaks at 329 nm and 423 nm can be found, which can be assigned to the 4f-5d transition of Sm^{2+}. The emission bands consist of a broad band emission from 550 to 650 nm with the peak at 603 nm. The sharp emission bands consists of three groups of lines at 683.5, 698 and 725.5 nm correspond to the $^5D_0\rightarrow{}^7F_0$, $^5D_0\rightarrow{}^7F_1$ and $^5D_0\rightarrow{}^7F_2$ transitions of Sm^{2+}, respectively. The strongest emission is at 698 ($^5D_0\rightarrow{}^7F_1$ of Sm^{2+}), which indicates that the Sm^{2+} ions occupy the crystallographic sites with central symmetry in the host.

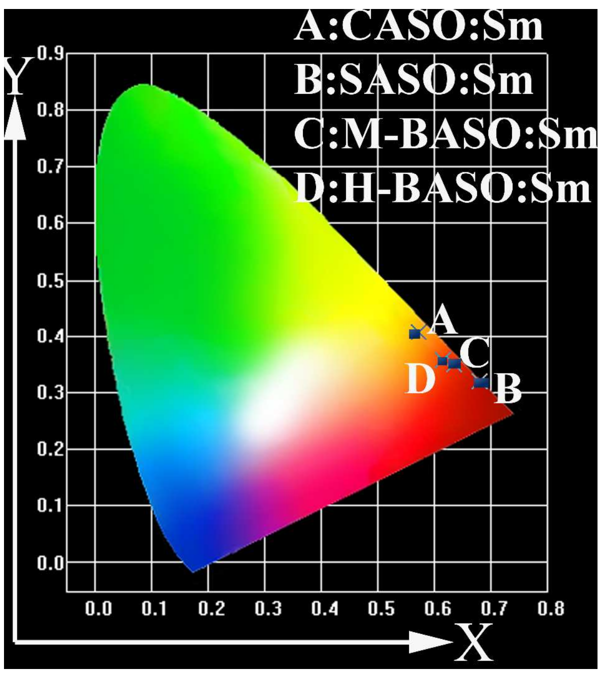

Figure 3. CIE (commission International de l'Ecairage 1931) chromaticity coordinates of Sm doped CASO, SASO, M-BASO and H-BASO.

Table 3. CIE values of Sm doped CASO, SASO, M-BASO and H-BASO.

Compound	CIE (excitation wavelength)
CASO:Sm	(0.573, 0.407) (374nm)
SASO:Sm	(0.680, 0.319) (360 nm)
M-BASO:Sm	(0.635, 0.350) (365nm)
H-BASO:Sm	(0.616, 0.357) (330 nm)

Figure 3 shows the CIE (commission International de I'Ecairage 1931) chromaticity coordinates of Sm doped CASO, SASO, M-BASO and H-BASO. For Sm-doped CASO, the emission light excited at 375 nm shows orange-red because it mainly comes from the emission of Sm^{3+}. For Sm doped SASO, M-BASO and H-BASO, as can be shown in Figure 2 and Table 3, excited at n-UV light, their CIE values are B(0.680, 0.319), C(0.635, 0.350) and D(0.616, 0.357), respectively. All of them yield strong deep red emission, which may be used as the red phosphors in the phosphors-converted light-emitting diodes.

4.2.2. **Crystal structure and spectra of Sm doped $MAl_2Si_2O_8$ (M=Ca, Sr, Ba)**

4.2.2.1. **The relationship between the crystal structure and the f-f transition intensity of Sm^{2+}**

From the above analysis, it has been clearly shown that the f-d transition energy of Sm doped SASO, M-BASO and H-BASO can produce f-d transition emission accompanied by some strong f-f transitions of Sm^{2+}, however, the f-f emission intensity are quite different. Their comparison of the emission intensity under the excitation of 360 or 460 nm can be shown in Figure 4. The clear order of the strongest f-f emission intensity of Sm^{2+} is H-BASO>>M-BASO＞SASO＞CASO. We will make our focus on the spectra analysis of Sm doped H-BASO, M-BASO and SASO to try to find out the relationship between the crystal structure and their PL properties because their strong f-d and f-f transition of Sm^{2+} at room temperature.

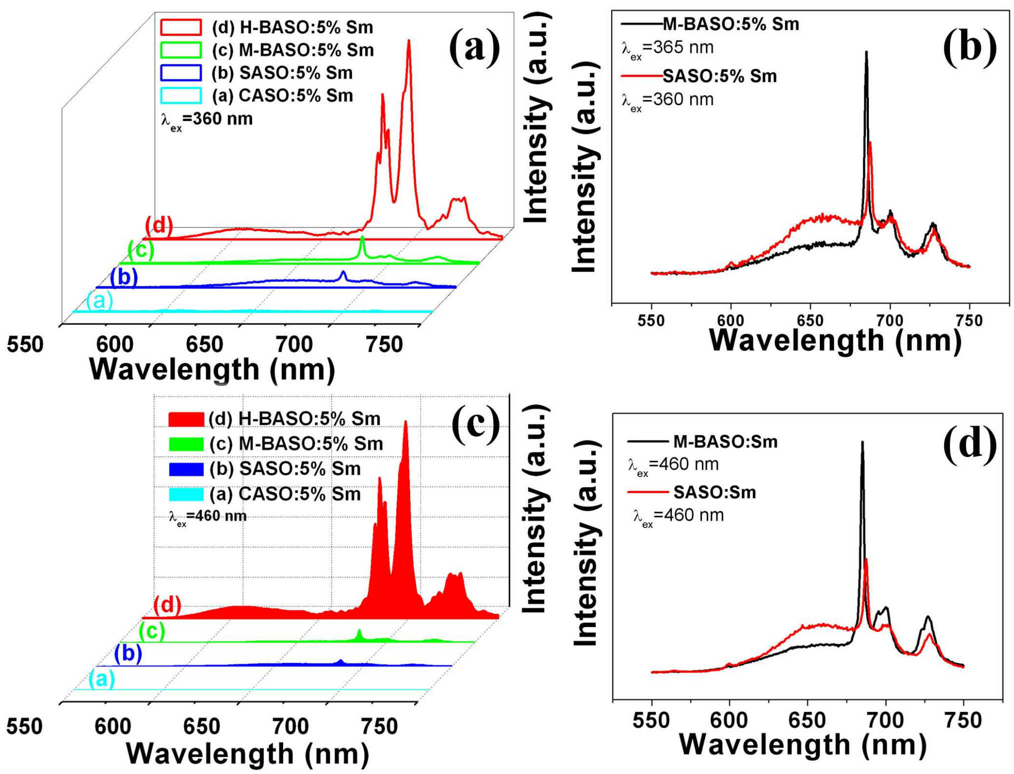

Figure 4. Comparison emission intensity of Sm doped CASO, SASO, M-BASO and H-BASO under the f-d transition energy excitation.

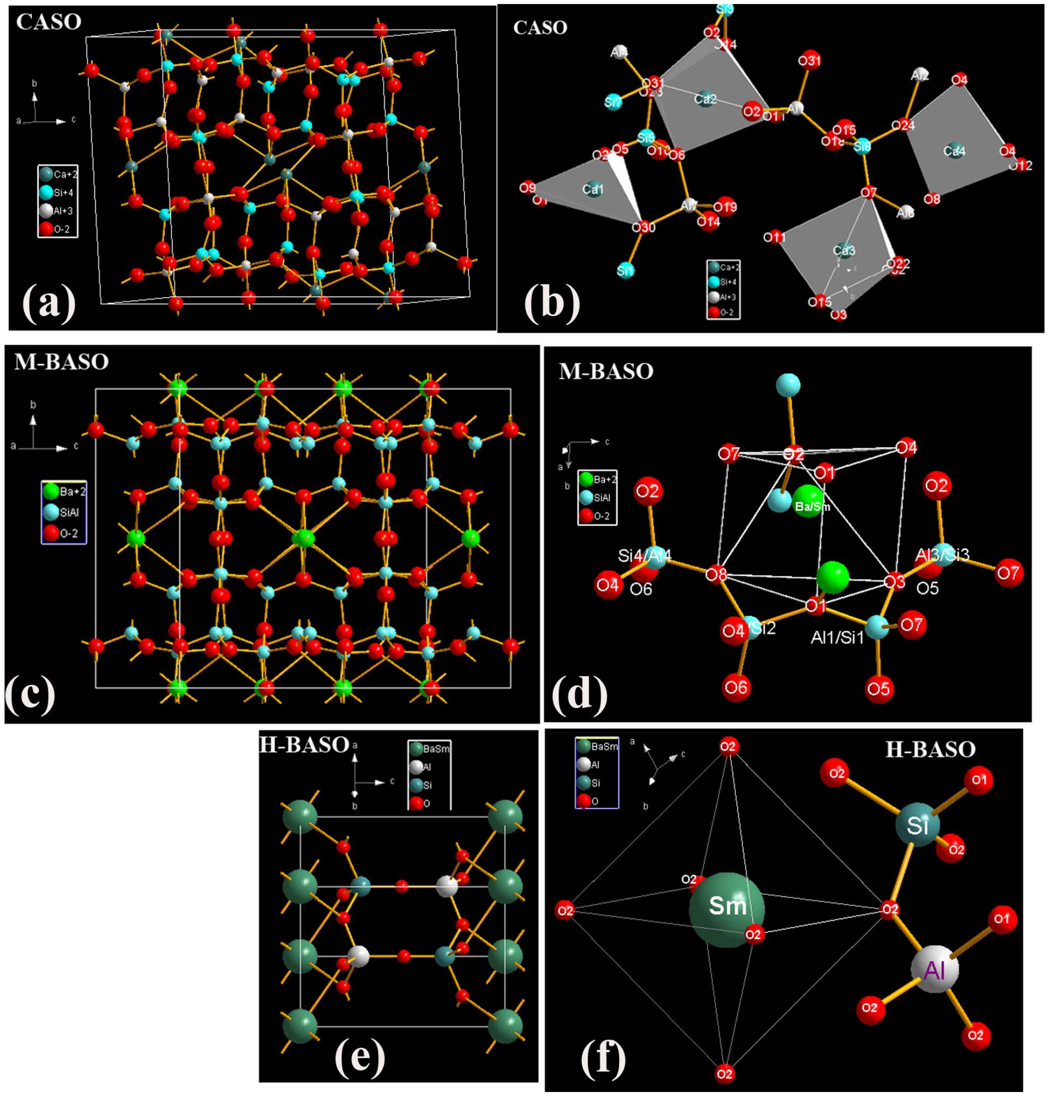

Figure 5. Crystal structure of Sm doped- CASO, M-BASO and H-BASO. (a), (c) and (e): Shape of the unit cell; (b), (d) and (f): Sm/Ca, Sm/ Ba-centred skeleton construction with nearest neighbor atoms, respectively. The detail structure data of CASO, M-BASO, SASO and H-BASO can be referred to references 16, 18, 17 and 4, respectively.

As is well known, the relative intensity of f-f transitions is influenced by the crystalline environment due to the different symmetry of the occupied sites[9, 10, 27-30]. The crystal structure of MASO(M=Ca and Ba) has been shown in Figure 5. In the Sm doped MASO (M=Ca and Ba) systematic samples, the Sm ions occupy the site of M^{2+} ions, therefore, the f-f transition intensity is mainly influenced by the symmetry of the M^{2+} sites. Just as the Eu^{3+} emission, the intensities of different $^5D_0$–^7F_J transitions of Sm^{2+} depend on the local symmetry of the crystal field of the Sm^{2+} ions[9-13]. The $^5D_0$–$^7F_0$ transition is hypersensitive, while the $^5D_0$–$^7F_1$ transition is insensitive to the crystal field environment. For instance, in a site with inversion symmetry, the $^5D_0$–$^7F_1$ transition is dominant, while in a site without inversion symmetry, the $^5D_0$–$^7F_0$ electronic transition becomes the strongest one. The intensity of $^5D_0$–$^7F_0$ transition is much higher than that of $^5D_0$–$^7F_1$, which is strong evidence that Sm^{2+} ions mainly occupy the lattice site without inversion symmetry[9]. From the crystal structure and the skeleton construction of MASO (Figure 5), we can see that only in the Sm-doped H-BASO sample, Sm occupy the centered site with six identity oxygens (O2), which is inversion symmetry, so the intensity of $^5D_0$–$^7F_1$ transition of Sm^{2+} in H-BASO is the strongest among the four samples.

The space groups of M-BASO and SASO are I 12/c1 (No. 15)[17, 18]. Both of the occupied sites of Ba^{2+} in M-BASO and Sr^{2+} in SASO are 8f. The symmetry of Ba^{2+} in M-BASO crystal is similar to that of Sr^{2+} in SASO crystal, but the intensity of $^5D_0$–$^7F_0$ transition of Sm^{2+} of M-BASO:Sm is about 2 time stronger than that of SASO:Sm, which can be shown in Figures 4(b) and 4d). In their crystal structure, as can be shown in Figures 5(c) and 5(d), there is one 8f site of Ba with seven different nearest neighbors atoms including two types of Ba-O1, one Ba-O2, one Ba-O3, one Ba-O4, one Ba-O7 and one Ba-O8 bonds. This type of symmetry produces the strong emission of the $^5D_0$–$^7F_0$ transition of Sm^{2+}. It has been found that the photoluminescence intensity ratio between $^5D_0\rightarrow{}^7F_2$ and $^5D_0\rightarrow{}^7F_1$ emission of Eu^{3+} ($I(^5D_0\rightarrow{}^7F_2)/I(^5D_0\rightarrow{}^7F_1)$) increases with increasing of the distortion degree of LnO_6 or LnO_7 polyhedron from that of an ideal octahedron. So, just as the Eu^{3+}, the transition intensity ratio between $^5D_0$–$^7F_0$ and $^5D_0$–$^7F_1$ emission of Sm^{2+} ($I(^5D_0\rightarrow{}^7F_0)/I(^5D_0\rightarrow{}^7F_1)$) is influenced by the distortion degree of LnO_n polyhedron from that of an ideal polyhedron[27, 28]. Their ratio values of $I(^5D_0\rightarrow{}^7F_0)/I(^5D_0\rightarrow{}^7F_1)$ for SASO:Sm, M-BASO and H-BASO are about 2.21, 3.34 and 0.95, respectively. The distortion degree can be calculated using the standard deviation of environmental factor of the individual bond (EFSD) $\sigma(h_{e_i})$, which can be expressed as below:

$$\sigma(h_{e_i}) = \sqrt{\frac{1}{N}\sum_{i=1}^{N}(h_{e_i} - \delta)^2} \qquad (11)$$

where $h_{e_i} = (f_c^{\mu}\alpha_b^{\mu})^{1/2} Q_B^{\mu}$ (12)

and $\delta = \frac{1}{N}\sum_{i=1}^{N} h_{e_i}$ (13)

Table 4. The environmental factor of any individual bond between the centre-M^{2+} atom and its nearest coordination atom (h_{e_i}) in the monoclinic crystals M-BASO and SASO, their standard deviation of the seven M-O environmental factors ($\sigma(h_{e_i})$) as well as the emission intensity ratio between $^5D_0\rightarrow{}^7F_0$ and $^5D_0\rightarrow{}^7F_1$ ($\frac{I(^5D_0\rightarrow{}^7F_0)}{I(^5D_0\rightarrow{}^7F_1)}$) in the hexagonal crystal H-BASO and

monoclinic crystals M-BASO and SASO.

Samples	Central ion	Bond type	f_c	α_b	Q_B	C.N.	h_{e_i}	$\sigma(h_{e_i})$	$\frac{I(^5D_0 \to ^7F_0)}{I(^5D_0 \to ^7F_1)}$
SASO	Sr^{2+}	Sr-O1	0.0318	0.1810	1.1429	2	0.08671	0.03379	2.21
		Sr-O2	0.0696	0.3123	0.8571	1	0.12636		
		Sr-O3	0.0650	0.5346	0.8571	1	0.15977		
		Sr-O4	0.0639	0.6209	0.8571	1	0.17072		
		Sr-O7	0.0646	0.5603	0.8571	1	0.16306		
		Sr-O8	0.0650	0.5306	0.8571	1	0.15917		
M-BASO	Ba^{2+}	Ba-O1	0.0304	0.2402	1.1429	2	0.09766	0.07348	3.34
		Ba-O2	0.0655	0.4451	0.8571	1	0.14635		
		Ba-O3	0.0626	0.6692	0.8571	1	0.20222		
		Ba-O4	0.0625	0.6809	0.8571	1	0.17681		
		Ba-O7	0.0628	0.6497	0.8571	1	0.17313		
		Ba-O8	0.0629	0.6437	0.8571	1	0.17246		
H-BASO	Ba^{2+}	Ba-O2	0.1047	1.1695	1.000	6	-	0	0.951

The related chemical parameters, such as the covalency f_c , the polarizability of the chemical bond volume α_b, and the present charge of the ligand in the binary crystals, are listed in Table 4. According to the equations (11)-(13), their standard deviation of the seven M-O environmental factors ($\sigma(h_{e_i})$) of MO_7 or MO_6 polyhedron in the SASO, M-BASO and H-BASO can be calculated to be 0.03379, 0.07348 and 0 respectively. The $\sigma(h_{e_i})$ value of M-BASO is 2.2 times larger than that of SASO. Generally, the $I(^5D_0\rightarrow{}^7F_0)/I(^5D_0\rightarrow{}^7F_1)$ value of Sm^{2+} increases with increasing of $\sigma(h_{e_i})$[27, 28]. Therefore, the $I(^5D_0\rightarrow{}^7F_0)/I(^5D_0\rightarrow{}^7F_1)$ of Sm^{2+} in the crystal M-BASO is stronger than that in the crystal SASO or H-BASO, and $I(^5D_0\rightarrow{}^7F_0)/I(^5D_0\rightarrow{}^7F_1)$ of H-BASO:Sm is the lowest.

4.2.2.2. **The relationship between the crystal structure and the f-d transition energy of Sm^{2+}**

Figure 6 shows the comparisons of 4f-5d transition excitation spectra in Sm^{2+} in H-BASO, M-BASO and SASO. (The intensity of H-BASO is reduced 6 times; and that of SASO is enlarged 1.5 times.) The lowest band comes from the Sm doped H-BASO (red line). The broad bands of Sm doped M-BASO and SASO have a blue-shift comparing with that of H-BASO. The 4f-5d transition band of Sm-SASO (blue line) has a blue-shift comparing with that of M-BASO (black line).

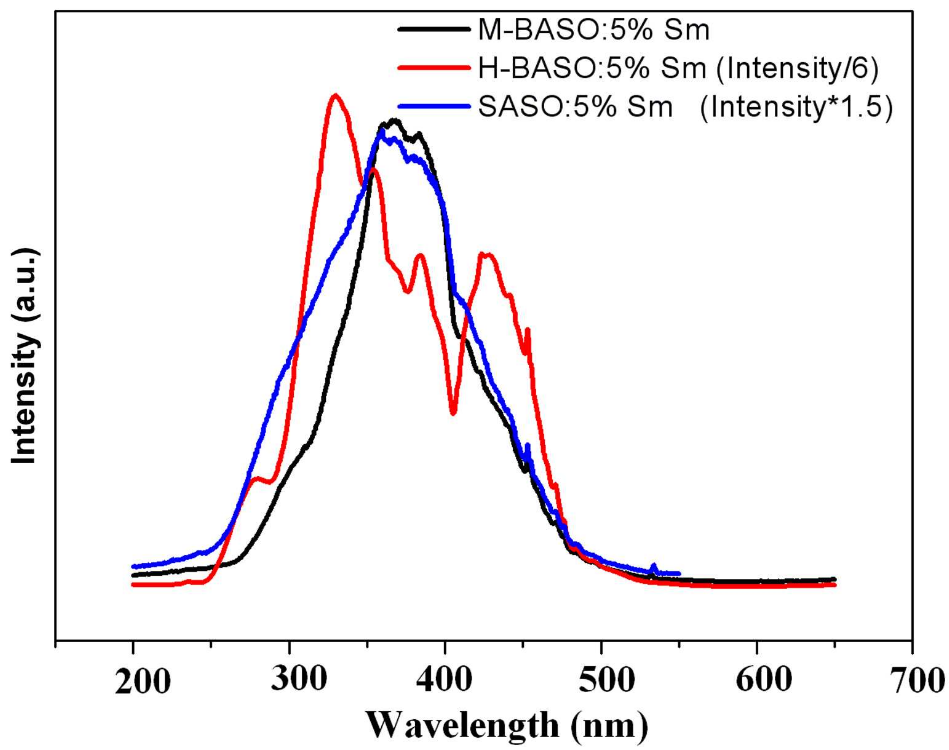

Figure 6. The 4f-5d transition excitation spectra of Sm^{2+} in H-BASO, M-BASO and SASO. (The intensity of H-BASO is reduced 6 times; and that of SASO is enlarged 1.5 times.) The lowest band comes from the Sm doped H-BASO(red line). The broad bands of Sm doped M-BASO and SASO have a blue-shift comparing with that of H-BASO. The 4f-5d transition band of Sm-SASO (blue line) has a blue shift comparing with that of M-BASO (black line).

As is well known, the 4f-5d transition energy is greatly influenced by the crystalline environmental[21, 22, 26, 31]. This is because that the excited states such as 5d are not shielded from the surrounding electronic shell, so the 5d electron has a strong interaction with the neighboring anions in the compound. The interactions for the $4f^5 5d$ configuration, which may be important for optical spectrum simulations, are as follows[32]:

$$H = H_0 + H_{coul}(ff) + H_{so}(f) + H_{cf}(f) + H_{cf}(d) + H_{so}(d) + H_{Coul}(fd) \qquad (14)$$

Where H_0 is the central-field interaction which includes the kinetic energy of electron and the Coulomb interaction between the $4f^5$ core and the electrons; $H_{coul}(ff)$, $H_{so}(f)$ and $H_{cf}(f)$ are Coulomb, spin-orbit and crystal-field interactions for the $4f^5$ core; $H_{cf}(d)$ and $H_{so}(d)$ are crystal field and spin orbit interactions for the single 5d electron; $H_{Coul}(fd)$ is the Coulomb interaction between the $4f^5$ core and the 5d electron. The order of magnitude of the energy splitting caused by these interactions is as follow:

$$H_0 \rangle \lfloor H_{Coul}(ff), H_{cf}(d) \rfloor \rangle H_{Coul}(fd) \rangle H_{so}(f) \rangle H_{so}(d) \rangle H_{cf}(f) \qquad (15)$$

The interactions $H_{so}(d)$ and $H_{cf}(f)$ can be generally ignored. In our systematic samples the central ion is Sm^{2+} with the electron $4f^6$ configuration, the lowest $4f^6 \rightarrow 4f^5 5d$ energy ($E_{\exp}(4f^6 - 4f^5 5d)$) is determined by five parts: the energy centroid of the 5d orbital (E_C), the Coulomb, spin-orbital interactions between 4f and 4f electrons ($E_{Coul}(ff), E_{so}(f)$), the Coulomb interactions between 4f and 5d electrons ($E_{coul}(fd)$) and the effect of the crystal field ($E_{cf}(d)$). Figure 7 shows a schematic energy diagram of the of $4f^6 \rightarrow 4f^5 5d$ configuration of Sm^{2+} in any host lattice.

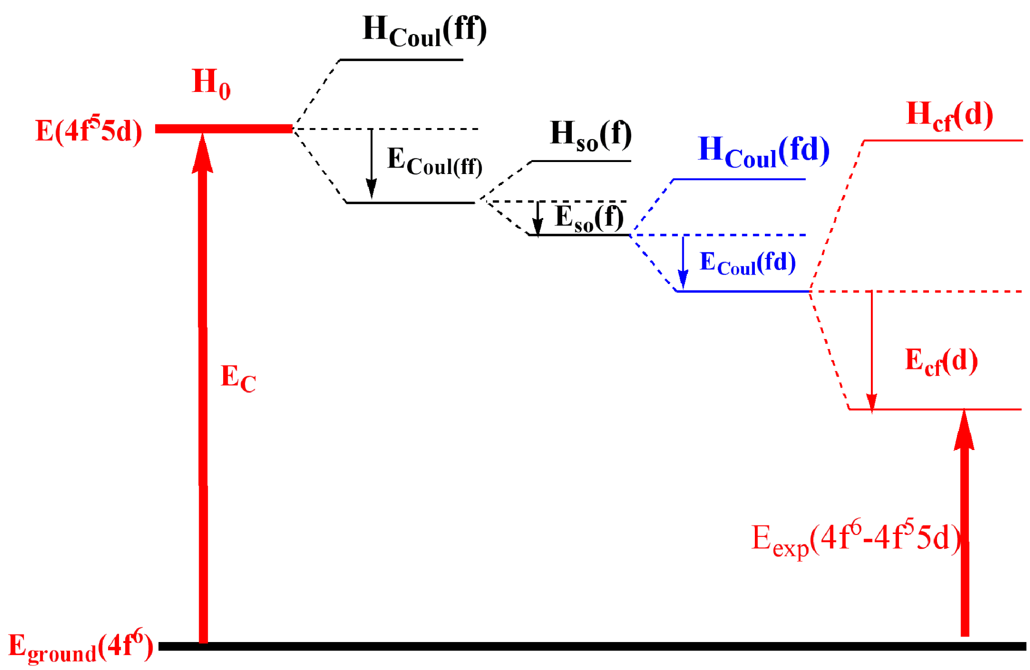

Figure 7. A schematic energy diagram of $4f^6 \rightarrow 4f^5 5d$ configuration of Sm^{2+} in any host lattice.

From the diagram (Figure 7) , the lowest $4f^6 \rightarrow 4f^5 5d$ transition energy of Sm^{2+} can be obtained as follows:

$$E_{\exp}(4f^6 - 4f^5 5d) = E_C - E_{Coul}(ff) - E_{so}(f) - E_{Coul}(fd) - E_{cf}(d) \quad (16)$$

In our case, all of the luminescence centre ions are Sm^{2+}, it is expected that $E_{Coul}(ff)$ and $E_{so}(f)$ are unchanged in the MASO (M=Sr and Ba) crystals. The energy difference among Sm-doped SASO, H-BASO and M-BASO mainly comes from the difference of the other three parts of equation (16): E_C, $E_{coul}(fd)$ and $E_{cf}(d)$. E_C and $E_{coul}(fd)$ are related to the environmental factor h_e [31] and $E_{cf}(d)$ is concerned with the environmental parameter F_C [22]. The values of h_e can be calculated using the below equations:

$$h_e = \left(\sum_{\mu} f_c^{\mu} \alpha_b^{\mu} Q_B^{\mu 2} \right)^{1/2} \quad (17)$$

Where Q_B^{μ} stands for the presented charge of the nearest anion in the chemical bond, and α_b^{μ} is the polarizability of the chemical bond volume in the μ type of chemical bonds[31]. Also, the relationship between the environmental factor (h_e) and the environmental factor of any individual bond between the centre atom and their nearest coordination atom (h_{e_i}) can be expressed by

$$h_e^2 = \sum_{i=1}^{N} \left(h_{e_i}^2 \right) \quad (18)$$

The values of the environmental parameter F_C can be obtained as follows:

$$F_C = \frac{\bar{E}_h \bar{Q} \bar{f}_i}{N} \quad (19)$$

Where $\bar{E}_h$ is the average homopolar part of the energy gap. $\bar{Q}$ is the average present charge of the anions, and $\bar{f}_i$ is the average bond ionicity between the central ion and the nearest neighbors.

According to the equations (18) and (19), the values of the environmental factor h_e and the environmental parameter F_C as well as their related chemical bond parameters are calculated and listed in Table 8. The h_e values of Sm doped H-BASO, M-BASO and SASO are 0.8573, 0.4028 and 0.3710, respectively. Generally, an increase of h_e leads to an decrease of the energy centroid of the 5d orbital (E_C)[31]. Thus the order of their E_C values is $E_C(H-BASO) \langle E_C(M-BASO) \langle E_C(SASO)$, and the order of the $E_{coul}(fd)$ value is just reverse[26]. It has been shown that the $E_{cf}(d)$ increases with increasing of F_C, so the order of the $E_{cf}(d)$ value is $E_{cf}(H-BASO)\rangle E_{cf}(SASO)\rangle E_{cf}(M-BASO)$. Finally, according to the equation (16), it can be judged that among the three samples the lowest 4f-5d transition energy of Sm doped H-BASO is the lowest, which coincides with the experimental data (423 nm). For the other two crystal M-BASO and SASO, their difference between the environmental factors (h_e) ($\Delta(h_e)$=0.0318) is near to the difference between F_C($\Delta(h_e)$=0.0553). On the other hand, the magnitude of H_0 is larger than others in equation (14). Thus the difference of the $E_{\exp}(4f^6-4f^5 5d)$ value is mainly demined by the difference of E_C, so the lowest 4f-5d energy of Sm-doped SASO is a little larger than that of Sm-doped M-BASO, which is consistent with the experimental result.

Table 5. the values of the corresponding crystal factors (F_C) and environmental factor (h_e) of the central ions M^{2+} for H-BASO, SASO and M-BASO samples.

Samples	Central ion	Bond type	E_h	f_i	Q_B	C.N.	F_C	h_e
SASO	Sr^{2+}	Sr-O1	3.4944	0.9682	1.1429	2	0.4278	0.3710
		Sr-O2	4.3145	0.9304	0.8571	1		
		Sr-O3	3.1692	0.9350	0.8571	1		
		Sr-O4	2.9126	0.9361	0.8571	1		
		Sr-O7	3.0862	0.9354	0.8571	1		
		Sr-O8	3.1828	0.9350	0.8571	1		
M-BASO	Ba^{2+}	Ba-O1	2.9564	0.9696	1.1429	2	0.3725	0.4028
		Ba-O2	3.4860	0.9345	0.8571	1		
		Ba-O3	2.7685	0.9374	0.8571	1		
		Ba-O4	2.7417	0.9375	0.8571	1		
		Ba-O7	2.8147	0.9372	0.8571	1		
		Ba-O8	2.8292	0.9371	0.8571	1		
		Ba-O2	2.9377	0.8953	1.000	6		
H-BASO	Ba^{2+}	Ba-O2	2.9377	0.8953	1.000	6	0.4384	0.8573

5. Conclusion

The Sm^{2+} doped triclinic $CaAl_2Si_2O_8$ (CASO), monoclinic $SrAl_2Si_2O_8$ (SASO) and $BaAl_2Si_2O_8$ (M-BASO) as well as hexagonal $BaAl_2Si_2O_8$(H-BASO) have been synthesized using polymerizable-complex technique under reducing atmosphere. At room temperature, under the N-UV or blue excitation, Sm^{2+} doped SASO, M-BASO and H-BASO showed strong red emission. Their strongest emission spectra mainly come from the $^5D_0 \rightarrow {}^7F_0$ transition of Sm^{2+} in the H-BASO crystal and the $^5D_0 \rightarrow {}^7F_1$ transition of Sm^{2+} in SASO and M-BASO, respectively. The calculated standard deviation of environmental factor of the individual bond of Sm disclosed the reason why the emission intensity ratio($I(^5D_0 \rightarrow {}^7F_0)/I(^5D_0 \rightarrow {}^7F_1)$) of Sm^{2+} in SASO is stronger than that in M-BASO and that of H-BASO is the lowest. The lowest excitation energy of 5d energy levels of Sm^{2+} have a blue-shift in the order H-BASO<M-BASO<SASO. The physical reason for spectral and energy level changes is analyzed in detail to be a comprehensive result from the shift of the energy centroid of the 5d orbital, the Coulomb interaction between 4f and 5d electrons, and the crystal-field splitting of 5d energy level. The theoretical analysis is in good agreement with our experimental result.

Acknowledgments

This work is financially supported by the National Natural Science

Foundations of China (Grant no. 21301053).

References

1. F. Clabau, A. Garcia, P. Bonville, D. Gonbeau, T. Le Mercier, P. Deniard and S. Jobic, *J. Solid State Chem.*, 2008, **181**, 1456.
2. W. B. Dai, *J. Mater. Chem. C*, 2014, **2**, 3951.
3. H. Guo, X. Y. Liu, F. Li, R. F. Wei, Y. L. Wei and C. Ma, *J. Electrochem. Soc.*, 2012, **159**, J223.
4. W. B. Im, Y.-I. Kim and D. Y. Jeon, *Chem. Mater.*, 2006, **18**, 1190.
5. M. Ma, D. Zhu, C. Zhao, T. Han, S. Cao and M. Tu, *Opt. Commun.*, 2012, **285**, 665.
6. Y. Wang, Z. Wang, P. Zhang, Z. Hong, X. Fan and G. Qian, *Mater. Lett.*, 2004, **58**, 3308.
7. C. Zhang, J. Yang, C. Lin, C. Li and J. Lin, *J. Solid State Chem.*, 2009, **182**, 1673.
8. Q. Zhang, X. Liu, Y. Qiao, B. Qian, G. Dong, J. Ruan, Q. Zhou, J. Qiu and D. Chen, *Opt. Mater.*, 2010, **32**, 427.
9. Y. Huang, W. Kai, K. Jang, H. S. Lee, X. Wang, Y. Zhang, D. Qin and C. Jiang, *Mater. Lett.*, 2008, **62**, 1913.
10. P. Mikhail, J. Hulliger, M. Schnieper and H. Bill, *J. Mater. Chem.*, 2000, **10**, 987.
11. M. Nogami and Y. Abe, *J. Appl. Phys.*, 1997, **81**, 6351.
12. Z. Pei, Q. Su and J. Zhang, *J. Alloys Compd.*, 1993, **198**, 51.

13. X. Wang, H. Riesen, M. A. Stevens-Kalceff and R. P. Rajan, *J. Phys. Chem. A*, 2014, **118**, 9445.

14. Q. Zeng, Z. Pei, S. Wang, Q. Su and S. Lu, *Chem. Mater.*, 1999, **11**, 605.

15. Q. Su, H. Liang, T. Hu, Y. Tao and T. Liu, *J. Alloys Compd.*, 2002, **344**, 132.

16. C. J. E. Kempster, H. D. Megaw and E. W. Radoslovich, *Acta Crystallogr.*, 1962, **15**, 1005.

17. P. Benna and E. Bruno, *Am. Mineral.*, 2001, **86**, 690.

18. R. E. Newnham and H. D. Megaw, *Acta Crystallogr. A*, 1960, **13**, 303.

19. J. Lin, M. Yu, C. Lin and X. Liu, *J. Phys. Chem. C*, 2007, **111**, 5835.

20. F. M. Gao, J. L. He, E. D. Wu, S. m. Liu, D. l. Yu, D. c. Li, S. Y. Zhang and Y. J. Tian, *Phys. Rev. Lett.*, 2003, **91**, 015502.

21. J. Shi and S. Zhang, *J. Phys.: Condens. Matter*, 2003, **15**, 4101.

22. J. S. Shi, Z. J. Wu, S. H. Zhou and S. Y. Zhang, *Chem. Phys. Lett.*, 2003, **380**, 245.

23. Z. J. Wu and S. Y. Zhang, *J. Phys. Chem. A*, 1999, **103**, 4270.

24. S. Y. Zhang, *Chemical Bond Theory of Complex Structure Crystals on Dielectric Description and Application* Science Publisher, Beijing, 2005.

25. L. Li and S. Y. Zhang, *J. Phys. Chem. B*, 2006, **110**, 21438.

26. Z. Fu, S. Zhou and S. Zhang, *J. Phys. Chem. B*, 2005, **109**, 14396.

27. L. Li, X. Liu, H. M. Noh, S. H. Park, J. H. Jeong and K. H. Kim, *J. Alloys Compd.*, 2015, **620**, 324.

28. L. Li, H. K. Yang, B. K. Moon, Z. Fu, C. Guo, J. H. Jeong, S. S. Yi, K. Jang and H. S. Le, *J. Phys. Chem. C*, 2009, **113**, 610.

29. J. G. Muller, J. Karthikeyan, P. Murugan and N. Lakshminarasimhan, *J. Phys. Chem. C*, 2014, **118**, 19308.

30. X. Zhang and H. J. Seo, *J. Alloys Compd.*, 2011, **509**, 2007.

31. J. S. Shi and S. Y. Zhang, *J. Phys. Chem. B*, 2004, **108**, 18845.

32. S. Y. Zhang, *Spectroscopy of Rare Earth Ions-Spectral property and Spectral Theory* Science Publisher, Beijing, 2008.